Lock-in Ultrafast Electron Microscopy Simultaneously Visualizes Carrier Recombination and Interface-Mediated Trapping

Garming, Mathijs W.H.; Bolhuis, Maarten; Conesa-Boj, Sonia; Kruit, Pieter; Hoogenboom, Jacob P.

DOI
10.1021/acs.jpclett.0c02345

Publication date
2020

Document Version
Final published version

Published in
The Journal of Physical Chemistry Letters

THE JOURNAL OF PHYSICAL CHEMISTRY Letters

pubs.acs.org/JPCL

Letter

Lock-in Ultrafast Electron Microscopy Simultaneously Visualizes Carrier Recombination and Interface-Mediated Trapping

Mathijs W. H. Garming,* Maarten Bolhuis, Sonia Conesa-Boj, Pieter Kruit, and Jacob P. Hoogenboom*

Cite This: *J. Phys. Chem. Lett.* 2020, 11, 8880−8886

Read Online

ACCESS | Metrics & More | Article Recommendations | Supporting Information

ABSTRACT: Visualizing charge carrier flow over interfaces or near surfaces meets great challenges concerning resolution and vastly different time scales of bulk and surface dynamics. Ultrafast or four-dimensional scanning electron microscopy (USEM) using a laser pump electron probe scheme circumvents the optical diffraction limit, but disentangling surface-mediated trapping and ultrafast carrier dynamics in a single measurement scheme has not yet been demonstrated. Here, we present lock-in USEM, which simultaneously visualizes fast bulk recombination and slow trapping. As a proof of concept, we show that the surface termination on GaAs, i.e., Ga or As, profoundly influences ultrafast movies. We demonstrate the differences can be attributed to trapping-induced surface voltages of approximately 100−200 mV, which is further supported by secondary electron particle tracing calculations. The simultaneous visualization of both competing processes opens new perspectives for studying carrier transport in layered, nanostructured, and two-dimensional semiconductors, where carrier trapping constitutes a major bottleneck for device efficiency.

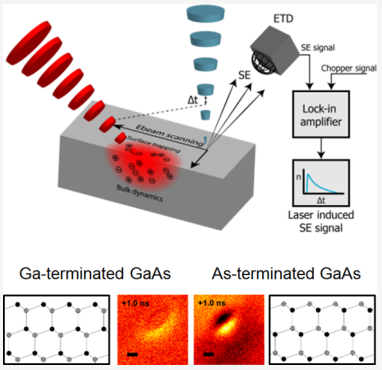

Observing and controlling the motion and recombination of excited charge carriers are keys to the functionality of semiconductor devices. Concomitant with miniaturization of device components, the relative contribution of trapping and recombination at surface or interface defects is increasing compared to that of bulk dynamics. Nevertheless, continuous miniaturization has so far been driving progress in many areas of technology, e.g., boosting computational power and clock speed in computer chips, increasing brightness and uniformity in lighting applications and displays, and enhancing efficiency in solar cells.[1−5] In fact, nanocomposite or nanostructured building blocks can now be found or have been proposed in many of these devices.[6−9] However, interface effects are becoming or, as in layered semiconductor solar cells, already are the main limitation of efficiency.[10−13]

Traditionally used optical techniques are incapable of meeting the nanometer-range resolution requirement to map the flow of charge carriers over interfaces, and further complications arise from bulk and surface dynamics occurring on time scales that can differ by orders of magnitude.[14−17] In ultrafast scanning electron microscopy (USEM), a focused electron beam is used to probe the dynamics of a charge carrier distribution after laser excitation, thus bringing electron beam resolution into the traditional pump−probe schemes.[18−21] With USEM, carrier dynamics has been studied in bulk materials such as Si and GaAs, in crystals including CIGSe and CdSe, and in layered materials like black phosphorus and across a silicon p−n junction.[22−31] In all schemes, low-energy, 0−10 eV, secondary electrons (SEs) are used as the probe signal. As these SEs typically have a very short, only a few nanometers, mean free path, the bulk contribution to the signal is naturally limited, leading to an exquisite sensitivity to surface-related phenomena.[32] Indeed, marked differences in subsurface carrier diffusivity for differently functionalized CdTe have recently been revealed using USEM.[33] However, the visualization of trapping at the surface together with the ultrafast carrier recombination dynamics has not been demonstrated. Visualizing trapped states is important for two reasons. First, highlighting where and the extent to which carrier trapping occurs allows for optimization of device fabrication and subsequent quality control, including surface cleaning and termination strategies. Second, trapped charges may lead to the occurrence of localized potentials that could, depending on their magnitude, in turn impact carrier transport and recombination near the interface. Directly decoupling ultrafast bulk dynamics and longer time-scale surface-induced trapping in USEM would thus provide more insight into the interplay between these competing mechanisms and thus aid further optimization of nanostructured semiconductor devices.

Here, we introduce lock-in secondary electron detection in USEM and show that it allows the detection of processes slower than the pump−probe repetition rate simultaneously with bulk relaxation. Thus, within the ultrafast movie, we can study the fast nanosecond-scale dynamics of the sample as a

Received: July 31, 2020
Accepted: September 10, 2020
Published: September 10, 2020

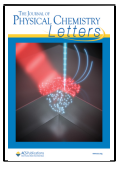

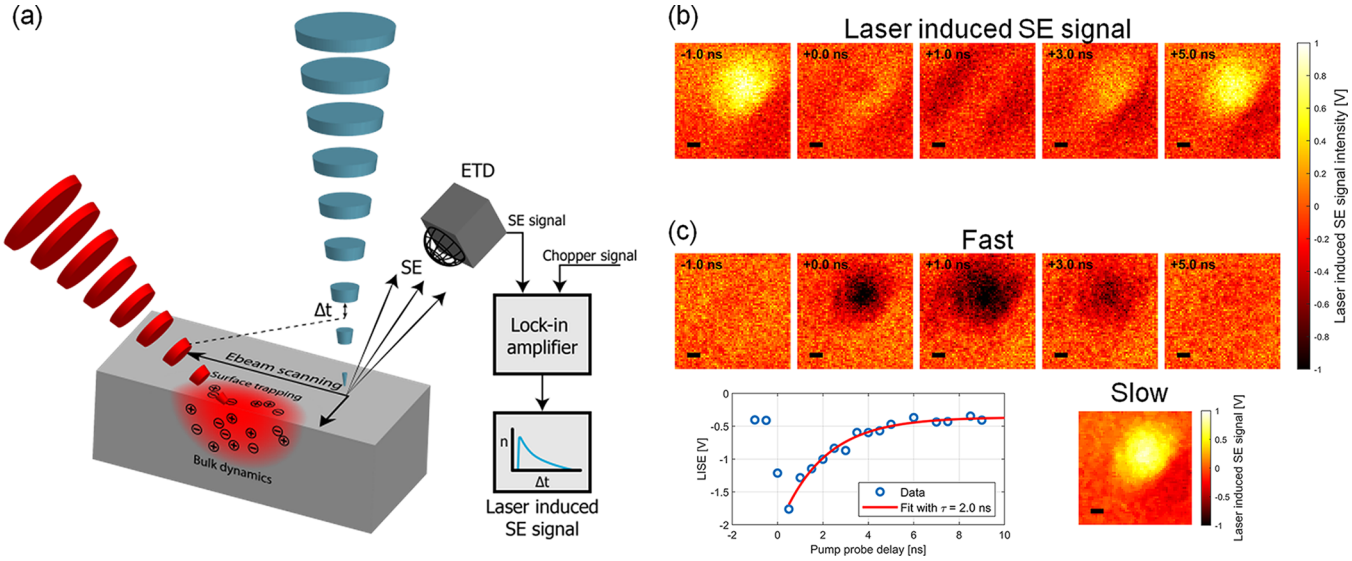

Figure 1. Lock-in USEM disentangles bulk recombination and surface trapping in GaAs from a single ultrafast measurement sequence. (a) In lock-in USEM, a laser pump electron probe scheme is used to map carrier dynamics through spatiotemporal variations in the secondary electron (SE) signal that are amplified through lock-in detection. (b) Scanning a GaAs (100) sample at various laser electron delays gives an ultrafast laser-induced SE image sequence. This shows the effect of carrier excitation at 0 ns on the SE yield, with the profile after ultrafast carrier relaxation matching that at negative times. (c) This movie can then be separated into the fast dynamics (<10 ns, top row) and slow relaxation processes, including carrier trapping (bottom right panel), allowing for data on both time scales to be acquired in a single measurement. The average intensity of the five darkest pixels in the fast dynamics figures decays single exponentially with a 2.0 ± 0.5 ns time constant, corresponding to the expected bulk carrier relaxation time of the material. Scale bars of 50 μm.

function of pump−probe delay, while the slow dynamics is imprinted in the longer pump−probe delays where the detector is effectively gated to remove the fast dynamics.

We use GaAs to illustrate our lock-in SEM. GaAs is a III−V semiconductor often used in optoelectronic applications, either directly or as a base material for further epitaxial growth of layered or nanoscale devices.[34] The GaAs interface has been well studied and exhibits a different landscape of trap states depending on the crystal orientation.[35,36] The (111) orientation in particular displays a smooth interface terminated with either a Ga or an As atomic layer.[34,37] The landscape of trap states on GaAs surfaces is known to give rise to the occurrence of surface voltages upon photoexcitation on the order of only 100−200 mV.[38] We will show that despite this small potential difference, our implementation of lock-in USEM reveals a marked difference in image contrast pattern between the (111)A and (111)B orientations. We will further show that this pattern formation can indeed be assigned to the slow, i.e., surface trapping-induced, component in carrier relaxation, while in both cases, the fast dynamics is governed by direct carrier recombination. We confirm our results through particle tracing simulations, electron spectroscopy, and direct sample current measurements. The ability to observe both trapping-induced localized voltages and ultrafast carrier transport underneath and around these locations may provide new avenues for inspection and optimization of semiconductor nanodevices and the study of carrier dynamics in and around interfaces.

In USEM, a pulsed laser beam excites electrons from the valence to the conduction band while a pulsed electron beam scans the sample at a set time delay with respect to the laser pulse. The presence of photoexcited charge carriers leads to a modification of the SE yield, which is probed by the electron pulse.[22,39] Through this laser-induced SE yield (LISE), i.e., the change in SE yield due to photoexcitation, the electron pulses thus probe the diffusion and relaxation of the excited carriers in time and space.

Our lock-in USEM setup (see also Figure 1a and Figure S1) combines a 95 MHz Coherent Vitara-T Ti:Sapph femtosecond laser at 800 nm with a pulsed electron beam (sub-100 ps at 4 keV[40]) in a FEI Quanta 200 FEG SEM instrument. Contrary to earlier implementations of USEM that have all required laser illumination of the electron source,[20,30,41] we use a standard commercial beam blanker to pulse our electron beam (see also section S1 of the Supporting Information and ref 40). Beam blankers are a well-established way to create pulsed electron beams[42−44] but have thus far not been applied to USEM systems. Moreover, we modulate the laser beam with a 940 Hz chopper and apply lock-in detection to directly extract the LISE signal from the SE detector (Figure 1a). While previous implementations relied on subtraction of long or negative time delay data to obtain the LISE signal,[21,28,29] this lock-in scheme ensures that any processes with a characteristic frequency between the pump−probe repetition frequency of 95 MHz and the 940 Hz chopping frequency will also be visible, on top of the ultrafast dynamic information. Additionally, the lock-in detection filters out minor drift-induced variations in the brightness of the image.

We illustrate our lock-in USEM acquisition in Figure 1 using (100)-oriented GaAs, cleaned immediately before being mounted in the USEM instrument (see section S2 of the Supporting Information). A bright laser-induced secondary electron (LISE) signal is observed in Figure 1b for pump−probe delays of 5−10 ns, i.e., approaching the inverse of our laser repetition frequency and, more importantly, much longer than the typical GaAs carrier lifetime of ∼2 ns.[45−47] Upon laser illumination, this bright spot instantly disappears, after which, with an increasing pump−probe delay, first dark side bands appear at Δt = 1 ns, followed by a gradual recovery of the bright signal. We attribute the persistent laser-induced

https://dx.doi.org/10.1021/acs.jpclett.0c02345
J. Phys. Chem. Lett. 2020, 11, 8880−8886

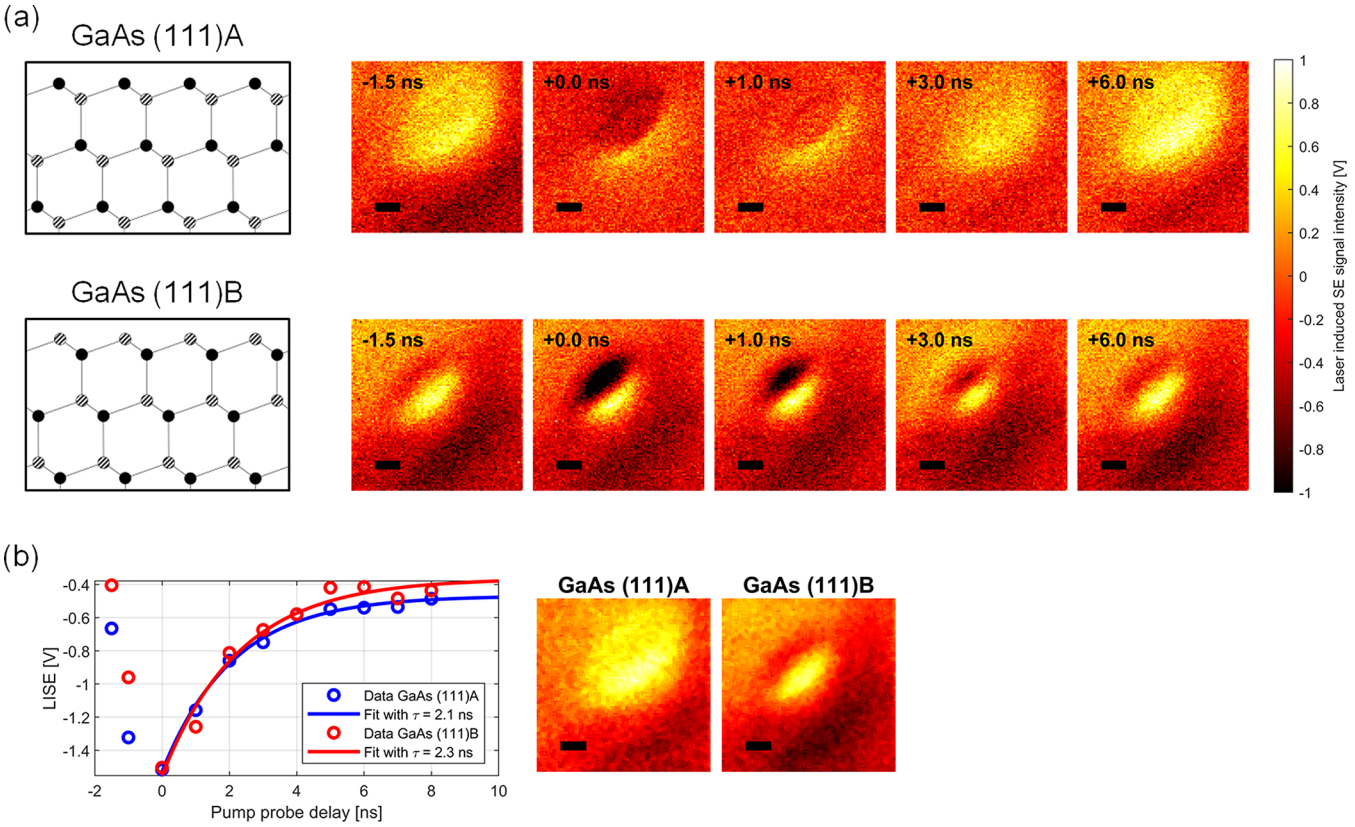

Figure 2. Visualization of trapping-induced contrast variations in ultrafast sequences of differently terminated GaAs (111). (a) GaAs (111) comes in a Ga-terminated A variant (top row) and an As-terminated B variant (bottom row), which display strikingly dissimilar ultrafast lock-in USEM image sequences, with a dipolar pattern appearing for the GaAs (111)B variant. In crystal structure images, solid-colored atoms correspond to Ga and dashed atoms to As. (b) Decomposing the videos in the slow components (images, right) and the ultrafast dynamics (graphed, left) in the same way as in Figure 1 reveals that the underlying bulk carrier lifetime is similar for both surfaces. Thus, the contrast differences originate from the slower processes and are attributed to different local surface voltages that develop due to carrier trapping but do not strongly affect the subsurface carrier lifetime. Scale bars of 50 μm.

enhancement of the SE signal that occurs long after laser pulse illumination to the trapping of photoexcited charge carriers at trap states on the GaAs surface.

GaAs surfaces are well-known for containing trap states that can have lifetimes significantly longer than our 10 ns pump−probe repetition rate.[46] We note that lock-in detection allows for their detection provided relaxation is faster than the 1 kHz laser chopping frequency. As we will show later, the presence of these trapped charges leads to an increase in the SE detection efficiency through the action of an induced local electric field at the vacuum side of the interface. We will refer to this surface trapping with a time constant in the range from 10 ns to 1 ms as the slow component in the carrier relaxation dynamics. Under the assumption that this slow component contributes equally to the LISE signal for all delays, we extract the fast dynamics by subtracting the long pump−probe delay image from all other images (Figure 1c). In this way, we obtain the typical dark contrast images previously reported for USEM on GaAs using the reference image subtraction technique.[22] Here, the dark contrast is seen to spread and return to the background signal on a 0−5 ns time scale. Plotting this fast LISE component versus delay time (Figure 1c), we indeed recover a single-exponential lifetime (τ) of 2.0 ± 0.5 ns, typical of bulk carrier recombination. Four other measurements on two additional chips resulted in lifetimes of 1.9, 1.9, 1.9, and 2.0 ns (data not shown). Note that the occurrence of the dark side bands in the LISE signal in Figure 1b at τ = 1 ns coincides with the maximal spreading of photoexcited carriers in the top row of Figure 1c. Thus, the two photoexcitation relaxation pathways of bulk recombination and trapping at surface defects both affect the LISE signal in qualitatively different ways and can, despite their different time scales, both be visualized in the same lock-in USEM measurements.

Surface composition and morphology can profoundly influence the nature of surface trap states;[35,36] as the (100) surface is known to be terraced containing a multitude of surface reconstructions over small length scales, we switch to the (111) orientation to illustrate this. The (111)-oriented GaAs crystal exists in a gallium-terminated variety termed GaAs (111)A and an arsenide-terminated variety termed GaAs (111)B.[34,37] The A and B variants thus have the same bulk structure but differ in their surface layer (Figure 2a) and thereby exhibit a different energy landscape at the interface. We perform USEM measurements on both GaAs (111)A and GaAs (111)B following the same cleaning procedure mentioned above (section S2 of the Supporting Information).

Our lock-in USEM gives a strikingly different appearance for the LISE images obtained on GaAs (111)A compared to those obtained on (111)B (Figure 2a). Where the (111)A Ga surface shows a bright spot for the longer time delays similar to that obtained for the GaAs (100) surface, the (111)B As surface has a markedly smaller and more elliptical high-intensity spot. Immediately after laser illumination, this difference becomes even more pronounced with the (111)B surface developing a

https://dx.doi.org/10.1021/acs.jpclett.0c02345
J. Phys. Chem. Lett. 2020, 11, 8880−8886

strong dipolar profile oriented perpendicular to the long axis of the laser illumination profile. The dark contrast lobe in this dipolar profile gradually diminishes with an increase in delay time. However, if, for both surfaces we subtract the slow component (image panels in Figure 2b) from the temporal dynamics like we did for the GaAs (100) above, we retrieve lifetimes of 2.1 and 2.3 ns for GaAs (111)A and GaAs (111)B, respectively (Figure 2b). An additional measurement on different chips gave values of 3.0 and 1.9 ns, respectively (data not shown). These ultrafast relaxation rates are reminiscent of bulk carrier recombination.

Despite the similarity of the underlying ultrafast carrier decay rate, the modulation of this ultrafast component with the persistent longer time-scale contribution gives rise to the even more dissimilar appearance of the LISE images for delays of a few nanoseconds, including the appearance of the dipolar contrast profile for GaAs (111)B. Like for GaAs (100), we attribute the slow component to carrier trapping at the GaAs−vacuum interface. This occupation of surface traps and the accompanying separation of charge carriers lead to the occurrence of a net surface potential.[38] The magnitude and sign of this surface potential depend on the density and energy levels of the trap states, which are different for different surface terminations and/or bulk crystal orientations. The surface potential in turn influences the trajectories of the low-energy secondary electrons,[48] leading to a surface potential-dependent LISE collection efficiency. To examine this in more detail, we show in Figure 3a diagonal cross sections for the intensity observed on the A and B surface lock-in USEM images at $\tau \approx 8$ ns. Asymmetric profiles are observed for both variants. The B variety shows a clear dip adjacent to a region of increased SE emission. This dip is slightly off center from the laser illumination spot. We note that this left side of the curve, and thus the top left corner of the LISE images in Figures 2 and 4, is the position that in our experimental configuration is closest to the location of the SE detector. The dip is absent in the A variety, but here a smaller LISE yield is also observed on the left side of the photoexcitation region. Both surface terminations therefore exhibit asymmetry in the LISE images but to a different degree, which we argue is due to a difference in surface potential.

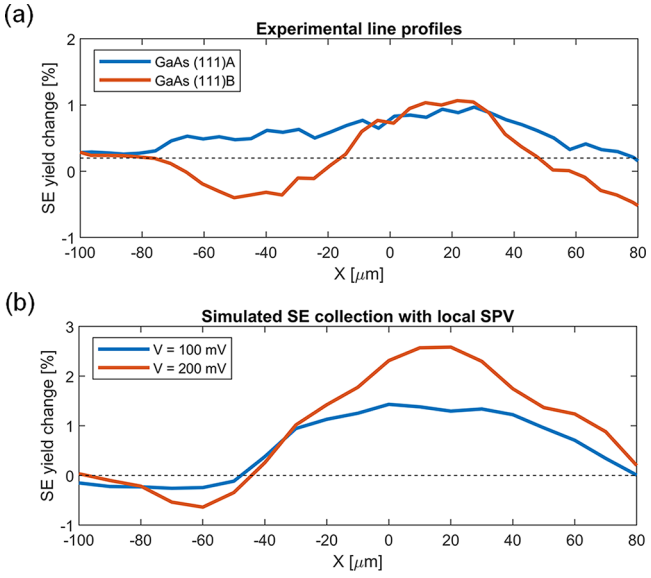

Figure 3. Trapping-induced local surface voltages lead to a spatially varying secondary electron collection yield that is responsible for the dipolar pattern on GaAs (111)B. (a) Diagonal cross section of laser-induced SE signal figures from top left to bottom right at an 8 ns pump−probe delay for GaAs (111)A and GaAs (111)B. For both curves, the number of SEs collected from the side of the laser spot closest to the detector is lowest. However, for the B variant, the contrast inversion is clearly visible; this is absent for the A variant. (b) Simulated SE collection efficiencies in the presence of a 100 and 200 mV Gaussian surface potential reproduce the dipolar contrast inversion when the surface voltage increases toward 200 mV.

We corroborate our interpretation of a surface potential-induced variation of collection efficiency with SE collection efficiencies obtained from particles tracing simulations in the presence of a 100−200 mV photoinduced surface potential (details of the simulation are given in section S3 of the Supporting Information). The calculated probability of SEs reaching the Everhart−Thornley detector (ETD) as a function of release position shows a marked similarity with our experimental results (Figure 3a,b). A surface potential of 100−200 mV already results in a clearly asymmetric, dipolar shape of SE collection efficiency. The calculated change in SE collection efficiency is on the order of a percent, comparable to the amplitude observed in the experiment. Thus, the dipolar contrast profile appears to be due to a combination of reabsorption of SEs and redirection of emitted SEs to the detector. As the ETD field is rather weak in the space between the grounded SEM pole piece and the sample (see also Figure S3a), many SEs are not sufficiently redirected and hit the pole piece instead of arriving at the ETD. Slowing these electrons with a local, positive surface potential partially prevents this from occurring. Moreover, SEs originating from the farther side of the laser illumination spot, as seen from the ETD, are not only slowed but also deflected toward the ETD by the surface potential. For electrons on the other side of the laser spot, the opposite occurs with the ETD field and surface potential field competing and thus creating a decrease in the SE collection efficiency in line with our experimental results. This surface potential-induced modulation of the SE collection efficiency is complementary to a possible change in SE yield, which is unrelated to the detector geometry and therefore intrinsically symmetric.

The surface potential of 100−200 mV corresponds to literature values of GaAs surface photovoltages that develop during continuous laser illumination.[49−53] On perovskites, surface photovoltages of ∼5 V arising from continuous laser illumination have been recently reported to influence SE trajectories to such an extent that a position-dependent collection efficiency can be observed.[48] We exclude the occurrence of localized surface potentials of this magnitude using a home-built retarding field analyzer (see section S4 of the Supporting Information). Here, a retarding field between sample and ETD prevents SEs with an energy smaller than the field magnitude from reaching the detector. The SE energy spectrum at each incident beam scan position is thus measured by varying the magnitude of the retarding field and collecting the transmitted electrons to construct an S curve. We observe no major shift in the curves obtained on laser-irradiated areas versus unirradiated areas on GaAs (111)B (Figure 4a,b), meaning the difference in surface potential is less than the sensitivity of the spectrometer, i.e., $\lesssim$250 mV. This is in stark contrast to calibration measurements using a biased copper wire that show clear curve shifts when an externally applied local potential is on the order of $\geq$1 V (figure S7). Finally, we

https://dx.doi.org/10.1021/acs.jpclett.0c02345
J. Phys. Chem. Lett. 2020, 11, 8880−8886

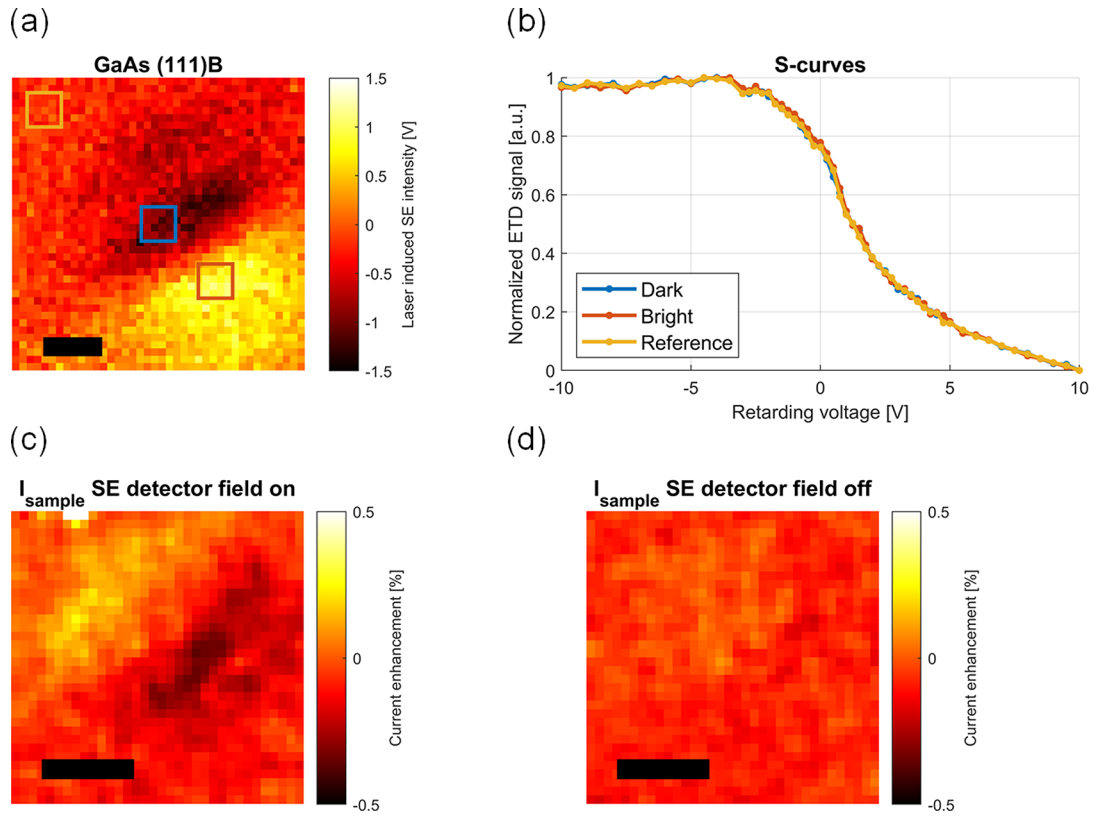

Figure 4. Retarding field spectral analyzer and direct sample current measurements confirm contrast variations are caused by small localized surface voltages. (a) Lock-in USEM result for GaAs (111)B with a 0 V retarding field on a grid placed above the sample. Regions of interest where the signal on the SE detector is monitored while the retarding voltage on the grid is varied are indicated with colored boxes. (b) For these regions, similar S curves are obtained, meaning the surface potential is <250 mV. (c) Measuring the current through the sample with the bias field on the SE detector switched on, we observe the contrast pattern inverted. (d) Switching the SE detector bias field off, we see the contrast pattern disappear, confirming the pattern is caused by an asymmetry in SE collection efficiency. Scale bars of 50 μm.

note that the observed asymmetry in the lock-in USEM images results from the combined action of the local surface potential and the ETD bias field that attracts the SEs. Indeed, if we measure the current through the sample as a function of scan position, the dipolar asymmetry disappears when the ETD bias field is switched off (Figure 4c,d). Thus, we conclude that lock-in USEM enables simultaneous visualization of photoexcited carrier relaxation via bulk recombination as well as trapping at energy states located at the interface.

The ability to see ultrafast carrier motion in relation to trapping-induced localized voltages provides new avenues for studying carrier transport in and across heterojunctions, underneath nanostructured surfaces, or at edges or layer transitions in two-dimensional materials. Locations for charge buildup can be directly visualized and related to changes in carrier recombination near the defect site. In the characterization of semiconductor nanodevices, lock-in USEM can enable the identification of spatial inhomogeneities that lead to trapping and thus aid the development of optimized fabrication processes and allow for quality control. Addition of an SE energy spectrum analyzer, like our initial retarding field analyzer, allows a direct evaluation of the magnitude of localized surface potentials, while the influence of the resulting internal field on charge dynamics can be monitored on time scales of nanoseconds or faster. We evaluated smooth interfaces, but localized impurities or defects that occur in fabrication may lead to larger local potentials. Lock-in USEM allows visualization of these fields, while their influence on local carrier transport can be simultaneously measured. Thus, we finally have the intriguing prospect of seeing charges move and recombine in and around the fields generated by trapped charges at high spatial and temporal resolution. This will ultimately aid the development of semiconductor nanodevices, for instance, in photovoltaics and photodetection, where the optimization of the ratio between bulk dynamics and surface trapping is crucial in optimizing device performance.

■ ASSOCIATED CONTENT

Supporting Information

The Supporting Information is available free of charge at https://pubs.acs.org/doi/10.1021/acs.jpclett.0c02345.

Further information about the setup and methodology, sample preparation, particle tracking simulations, and the retarding field analyzer (PDF)

■ AUTHOR INFORMATION

Corresponding Authors

Mathijs W. H. Garming − *Department of Imaging Physics, Delft University of Technology, 2628 CN Delft, The Netherlands*; Email: m.w.h.garming@tudelft.nl

Jacob P. Hoogenboom − *Department of Imaging Physics, Delft University of Technology, 2628 CN Delft, The Netherlands*; orcid.org/0000-0003-4539-8772; Email: j.p.hoogenboom@tudelft.nl

https://dx.doi.org/10.1021/acs.jpclett.0c02345
J. Phys. Chem. Lett. 2020, 11, 8880−8886

Authors

Maarten Bolhuis − *Kavli Institute of Nanoscience, Delft University of Technology, 2628 CJ Delft, The Netherlands*

Sonia Conesa-Boj − *Kavli Institute of Nanoscience, Delft University of Technology, 2628 CJ Delft, The Netherlands;* orcid.org/0000-0003-1716-184X

Pieter Kruit − *Department of Imaging Physics, Delft University of Technology, 2628 CN Delft, The Netherlands*

Complete contact information is available at: https://pubs.acs.org/10.1021/acs.jpclett.0c02345

Author Contributions

M.W.H.G. performed all experiments, sample preparation, and analysis. M.B. and S.C.-B. performed the EDX TEM experiments. M.W.H.G., P.K., and J.P.H. interpreted the data. M.W.H.G. and J.P.H. wrote the manuscript, with input from S.C.-B. and P.K. All authors agreed on the final version. P.K. and J.P.H. supervised the work. J.P.H. initiated the project. Experiments were conceived and designed by M.W.H.G., P.K., and J.P.H. S.C.-B. suggested the use of GaAs(111).

Notes

The authors declare no competing financial interest.

■ ACKNOWLEDGMENTS

The authors thank Gerward Weppelman for his help in the construction of the setup and initial experiments and Daan Brinks for a critical reading of the manuscript. M.B. and S.C.-B. acknowledge financial support from ERC through Starting Grant "TESLA" Grant Agreement 805021.

■ REFERENCES

(1) Franklin, A. D. Nanomaterials in transistors: From high-performance to thin-film applications. *Science* **2015**, *349*, aab2750.

(2) Epicoco, M. Knowledge patterns and sources of leadership: Mapping the semiconductor miniaturization trajectory. *Research Policy* **2013**, *42*, 180−195.

(3) Chen, B.; Pradhan, N.; Zhong, H. From large-scale synthesis to lighting device applications of ternary I-III-VI semiconductor nanocrystals: Inspiring greener material emitters. *J. Phys. Chem. Lett.* **2018**, *9*, 435−445.

(4) Yu, R.; Lin, Q.; Leung, S. F.; Fan, Z. Nanomaterials and nanostructures for efficient light absorption and photovoltaics. *Nano Energy* **2012**, *1*, 57−72.

(5) Guzelturk, B.; Martinez, P. L. H.; Zhang, Q.; Xiong, Q.; Sun, H.; Sun, X. W.; Govorov, A. O.; Demir, H. V. Excitonics of semiconductor quantum dots and wires for lighting and displays. *Laser and Photonics Reviews* **2014**, *8*, 73−93.

(6) Yang, P.; Yan, R.; Fardy, M. Semiconductor nanowire: Whats next? *Nano Lett.* **2010**, *10*, 1529−1536.

(7) Lopez-Sanchez, O.; Lembke, D.; Kayci, M.; Radenovic, A.; Kis, A. Ultrasensitive photodetectors based on monolayer MoS 2. *Nat. Nanotechnol.* **2013**, *8*, 497−501.

(8) Van Dam, D.; Abujetas, D. R.; Paniagua-Domínguez, R.; Sánchez-Gil, J. A.; Bakkers, E. P.; Haverkort, J. E.; Gómez Rivas, J. Directional and polarized emission from nanowire arrays. *Nano Lett.* **2015**, *15*, 4557−4563.

(9) Gibson, S. J.; van Kasteren, B.; Tekcan, B.; Cui, Y.; van Dam, D.; Haverkort, J. E.; Bakkers, E. P.; Reimer, M. E. Tapered InP nanowire arrays for efficient broadband high-speed single-photon detection. *Nat. Nanotechnol.* **2019**, *14*, 473−479.

(10) Cui, Y.; Wang, J.; Plissard, S. R.; Cavalli, A.; Vu, T. T.; Van Veldhoven, R. P.; Gao, L.; Trainor, M.; Verheijen, M. A.; Haverkort, J. E.; et al. Efficiency enhancement of InP nanowire solar cells by surface cleaning. *Nano Lett.* **2013**, *13*, 4113−4117.

(11) Kim, S. Y.; Rana, T. R.; Kim, J. H.; Son, D. H.; Yang, K. J.; Kang, J. K.; Kim, D. H. Limiting effects of conduction band offset and defect states on high efficiency CZTSSe solar cell. *Nano Energy* **2018**, *45*, 75−83.

(12) Haverkort, J. E.; Garnett, E. C.; Bakkers, E. P. Fundamentals of the nanowire solar cell: Optimization of the open circuit voltage. *Appl. Phys. Rev.* **2018**, *5*, 031106.

(13) Holm, J. V.; Jørgensen, H. I.; Krogstrup, P.; Nygård, J.; Liu, H.; Aagesen, M. Surface-passivated GaAsP single-nanowire solar cells exceeding 10% efficiency grown on silicon. *Nat. Commun.* **2013**, *4*, 1498.

(14) Haight, R. Electron dynamics at surfaces. *Surf. Sci. Rep.* **1995**, *21*, 275−325.

(15) Yang, Y.; Yang, M.; Moore, D. T.; Yan, Y.; Miller, E. M.; Zhu, K.; Beard, M. C. Top and bottom surfaces limit carrier lifetime in lead iodide perovskite films. *Nat. Energy* **2017**, *2*, 16207.

(16) Pattengale, B.; Huang, J. Implicating the contributions of surface and bulk states on carrier trapping and photocurrent performance of BiVO4 photoanodes. *Phys. Chem. Chem. Phys.* **2017**, *19*, 6831−6837.

(17) Shaheen, B. S.; El-Zohry, A. M.; Yin, J.; De Bastiani, M.; De Wolf, S.; Bakr, O. M.; Mohammed, O. F. Visualization of charge carrier trapping in silicon at the atomic surface level using four-dimensional electron imaging. *J. Phys. Chem. Lett.* **2019**, *10*, 1960−1966.

(18) Yang, D. S.; Liao, B.; Mohammed, O. F. Scanning ultrafast electron microscopy: Four-dimensional imaging of materials dynamics in space and time. *MRS Bull.* **2018**, *43*, 491−496.

(19) Zewail, A. H. Four-dimensional electron microscopy. *Science* **2010**, *328*, 187−193.

(20) Mohammed, O. F.; Yang, D. S.; Pal, S. K.; Zewail, A. H. 4D scanning ultrafast electron microscopy: Visualization of materials surface dynamics. *J. Am. Chem. Soc.* **2011**, *133*, 7708−7711.

(21) Liao, B.; Najafi, E. Scanning ultrafast electron microscopy: A novel technique to probe photocarrier dynamics with high spatial and temporal resolutions. *Materials Today Physics* **2017**, *2*, 46−53.

(22) Cho, J.; Hwang, T. Y.; Zewail, A. H. Visualization of carrier dynamics in p(n)-type GaAs by scanning ultrafast electron microscopy. *Proc. Natl. Acad. Sci. U. S. A.* **2014**, *111*, 2094−2099.

(23) Bose, R.; Bera, A.; Parida, M. R.; Adhikari, A.; Shaheen, B. S.; Alarousu, E.; Sun, J.; Wu, T.; Bakr, O. M.; Mohammed, O. F. Real-space mapping of surface trap states in CIGSe nanocrystals using 4D electron microscopy. *Nano Lett.* **2016**, *16*, 4417−4423.

(24) Liao, B.; Najafi, E.; Li, H.; Minnich, A. J.; Zewail, A. H. Photo-excited hot carrier dynamics in hydrogenated amorphous silicon imaged by 4D electron microscopy. *Nat. Nanotechnol.* **2017**, *12*, 871−876.

(25) Liao, B.; Zhao, H.; Najafi, E.; Yan, X.; Tian, H.; Tice, J.; Minnich, A. J.; Wang, H.; Zewail, A. H. Spatial-temporal imaging of anisotropic photocarrier dynamics in black phosphorus. *Nano Lett.* **2017**, *17*, 3675−3680.

(26) Shaheen, B. S.; Sun, J.; Yang, D. S.; Mohammed, O. F. Spatiotemporal observation of electron-impact dynamics in photovoltaic materials using 4D electron microscopy. *J. Phys. Chem. Lett.* **2017**, *8*, 2455−2462.

(27) Yang, D. S.; Mohammed, O. F.; Zewail, A. H. Environmental scanning ultrafast electron microscopy: Structural dynamics of solvation at interfaces. *Angew. Chem., Int. Ed.* **2013**, *52*, 2897−2901.

(28) Najafi, E.; Scarborough, T. D.; Tang, J.; Zewail, A. Four-dimensional imaging of carrier interface dynamics in p−n junctions. *Science* **2015**, *347*, 164−167.

(29) Najafi, E.; Ivanov, V.; Zewail, A.; Bernardi, M. Super-diffusion of excited carriers in semiconductors. *Nat. Commun.* **2017**, *8*, 15177.

(30) Zani, M.; Sala, V.; Irde, G.; Pietralunga, S. M.; Manzoni, C.; Cerullo, G.; Lanzani, G.; Tagliaferri, A. Charge dynamics in aluminum oxide thin film studied by ultrafast scanning electron microscopy. *Ultramicroscopy* **2018**, *187*, 93−97.

(31) Bose, R.; Sun, J.; Khan, J. I.; Shaheen, B. S.; Adhikari, A.; Ng, T. K.; Burlakov, V. M.; Parida, M. R.; Priante, D.; Goriely, A.; et al. Real-

space visualization of energy loss and carrier diffusion in a semiconductor nanowire array using 4D electron microscopy. *Adv. Mater.* **2016**, *28*, 5106−5111.
(32) Reimer, L. *Scanning electron microscopy*; Springer: Berlin, 1998; pp 135−169.
(33) El-Zohry, A. M.; Shaheen, B. S.; Burlakov, V. M.; Yin, J.; Hedhili, M. N.; Shikin, S.; Ooi, B.; Bakr, O. M.; Mohammed, O. F. Extraordinary carrier diffusion on CdTe surfaces uncovered by 4D electron microscopy. *Chem.* **2019**, *5*, 706−718.
(34) Moll, N.; Kley, A.; Pehlke, E.; Scheffler, M. GaAs equilibrium crystal shape from first principles. *Phys. Rev. B: Condens. Matter Mater. Phys.* **1996**, *54*, 8844−8855.
(35) Joyce, H. J.; Parkinson, P.; Jiang, N.; Docherty, C. J.; Gao, Q.; Tan, H. H.; Jagadish, C.; Herz, L. M.; Johnston, M. B. Electron mobilities approaching bulk limits in "surface-free;; GaAs nanowires. *Nano Lett.* **2014**, *14*, 5989−5994.
(36) Demichel, O.; Heiss, M.; Bleuse, J.; Mariette, H.; Fontcuberta i Morral, A. Impact of surfaces on the optical properties of GaAs nanowires. *Appl. Phys. Lett.* **2010**, *97*, 201907.
(37) Brozel, M.; Stillman, G. *Properties of gallium arsenide*, 3rd ed.; Institution of Engineering and Technology, 1996; pp 145−149.
(38) Kronik, L.; Shapira, Y. Surface photovoltage spectroscopy of semiconductor structures: At the crossroads of physics, chemistry and electrical engineering. *Surf. Interface Anal.* **2001**, *31*, 954−965.
(39) Sun, J.; Adhikari, A.; Shaheen, B. S.; Yang, H.; Mohammed, O. F. Mapping carrier dynamics on material surfaces in space and time using scanning ultrafast electron microscopy. *J. Phys. Chem. Lett.* **2016**, *7*, 985−994.
(40) Moerland, R. J.; Weppelman, I. G. C.; Garming, M. W. H.; Kruit, P.; Hoogenboom, J. P. Time-resolved cathodoluminescence microscopy with sub-nanosecond beam blanking for direct evaluation of the local density of states. *Opt. Express* **2016**, *24*, 24760.
(41) Sun, J.; Melnikov, V. A.; Khan, J. I.; Mohammed, O. F. Real-space imaging of carrier dynamics of materials surfaces by second-generation four-dimensional scanning ultrafast electron microscopy. *J. Phys. Chem. Lett.* **2015**, *6*, 3884−3890.
(42) MacDonald, N. C.; Robinson, G. Y.; White, R. M. Time-resolved scanning electron microscopy and its application to bulk-effect oscillators. *J. Appl. Phys.* **1969**, *40*, 4516−4528.
(43) Robinson, G. Y. Stroboscopic scanning electron microscopy at Gigahertz frequencies. *Rev. Sci. Instrum.* **1971**, *42*, 251−255.
(44) Ura, K.; Fujioka, H.; Hosokawa, T. Picosecond pulse stroboscopic scanning electron microscope. *J. Electron Microsc.* **1978**, *27*, 247−252.
(45) Beard, M. C.; Turner, G. M.; Schmuttenmaer, C. A. Transient photoconductivity in GaAs as measured by time-resolved terahertz spectroscopy. *Phys. Rev. B: Condens. Matter Mater. Phys.* **2000**, *62*, 15764−15777.
(46) Walker, A. W.; Heckelmann, S.; Karcher, C.; Höhn, O.; Went, C.; Niemeyer, M.; Bett, A. W.; Lackner, D. Nonrad iative lifetime extraction using power-dependent relative photoluminescence of III-V semiconductor double-heterostructures. *J. Appl. Phys.* **2016**, *119*, 155702.
(47) Weiner, J. S.; Yu, P. Y. Free carrier lifetime in semi-insulating GaAs from time-resolved band-to-band photoluminescence. *J. Appl. Phys.* **1984**, *55*, 3889−3891.
(48) Irde, G.; Pietralunga, S. M.; Sala, V.; Zani, M.; Ball, J. M.; Barker, A. J.; Petrozza, A.; Lanzani, G.; Tagliaferri, A. Imaging photoinduced surface potentials on hybrid perovskites by real-time Scanning Electron Microscopy. *Micron* **2019**, *121*, 53−65.
(49) Burstein, L.; Bregman, J.; Shapira, Y. Characterization of interface states at III-V compound semiconductor-metal interfaces. *J. Appl. Phys.* **1991**, *69*, 2312−2316.
(50) Łagowski, J.; Baltov, I.; Gatos, H. C. Surface photovoltage spectroscopy and surface piezoelectric effect in GaAs. *Surf. Sci.* **1973**, *40*, 216−226.
(51) Marshall, G. M.; Lopinski, G. P.; Bensebaa, F.; Dubowski, J. J. Electro-optic investigation of the surface trapping efficiency in n-alkanethiol SAM passivated GaAs(001). *Nanotechnology* **2011**, *22*, 235704.
(52) Siffalovic, P.; Drescher, M.; Heinzmann, U. Femtosecond time-resolved core-level photoelectron spectroscopy tracking surface photovoltage transients on p − GaAs. *Europhysics Letters (EPL)* **2002**, *60*, 924−930.
(53) Mao, D.; Kahn, A.; LeLay, G.; Marsi, M.; Hwu, Y.; Margaritondo, G.; Santos, M.; Shayegan, M.; Florez, L. T.; Harbison, J. P. Surface photovoltage and band bending at metal/GaAs interfaces: A contact potential difference and photoemission spectroscopy study. *J. Vac. Sci. Technol., B: Microelectron. Process. Phenom.* **1991**, *9*, 2083−2089.

https://dx.doi.org/10.1021/acs.jpclett.0c02345
J. Phys. Chem. Lett. 2020, 11, 8880−8886